MONTANA STATE UNIVERSITY LIBRARY

Emerging role of wetland methane emissions in driving 21st century climate change

Authors: Zhen Zhang, Niklaus E. Zimmermann, Andrea Stenke, Xin Li, Elke L. Hodson, Gaofeng Zhu, Chunlin Huang, and Benjamin Poulter

This is a postprint of an article that originally appeared in Proceedings of the National Academy of Sciences of the United States of America on September 5, 2017. The final version can be found at https://dx.doi.org/10.1073/pnas.1618765114.

Zhang, Zhen, Niklaus E. Zimmermann, Andrea Stenke, Xin Li, Elke L. Hodson, Gaofeng Zhu, Chunlin Huang, and Benjamin Poulter. "Emerging role of wetland methane emissions in driving 21st century climate change." Proceedings of the National Academy of Sciences of the United States of America 114, no. 36 (September 2017): 9647-9652. DOI: 10.1073/pnas.1618765114]

Made available through Montana State University's ScholarWorks
scholarworks.montana.edu

Emerging role of wetland methane emissions in driving 21st century climate change

Zhen Zhang[a,b,c,1], Niklaus E. Zimmermann[a,d], Andrea Stenke[d], Xin Li[c,e], Elke L. Hodson[f], Gaofeng Zhu[g], Chunlin Huang[c], and Benjamin Poulter[c,h]

[a]Dynamic Macroecology, Swiss Federal Research Institute WSL, Birmensdorf 8903, Switzerland; [b]Institute on Ecosystems and Department of Ecology, Montana State University, Bozeman, MT 59717; [c]Northwest Institute of Eco-Environment and Resources, Chinese Academy of Sciences, Lanzhou 730000, China; [d]Department of Environmental System Science, ETH Zürich, Zürich 8092, Switzerland; [e]CAS Center for Excellence in Tibetan Plateau Earth Sciences, Chinese Academy of Sciences, Beijing 100101, China; [f]Office of Energy Policy and Systems Analysis, US Department of Energy, Washington, DC 20585; [g]Key Laboratory of Western China's Environmental Systems, Lanzhou University, Lanzhou 730000, China; and [h]Biospheric Sciences Laboratory, NASA Goddard Space Flight Center, Greenbelt, MD 20770

Edited by Wolfgang Lucht, Potsdam Institute of Climate Impact Research, Potsdam, Germany, and accepted by Editorial Board Member Hans J. Schellnhuber July 26, 2017 (received for review November 12, 2016)

Wetland methane (CH_4) emissions are the largest natural source in the global CH_4 budget, contributing to roughly one third of total natural and anthropogenic emissions. As the second most impor-tant anthropogenic greenhouse gas in the atmosphere after CO_2, CH_4 is strongly associated with climate feedbacks. However, due to the paucity of data, wetland CH_4 feedbacks were not fully assessed in the Intergovernmental Panel on Climate Change Fifth Assessment Report. The degree to which future expansion of wetlands and CH_4 emissions will evolve and consequently drive climate feedbacks is thus a question of major concern. Here we present an ensemble estimate of wetland CH_4 emissions driven by 38 general circulation models for the 21st century. We find that climate change-induced increases in boreal wetland extent and temperature-driven increases in tropical CH_4 emissions will dominate anthropogenic CH_4 emissions by 38 to 56% toward the end of the 21st century under the Representative Concentration Pathway (RCP2.6). Depending on scenarios, wetland CH_4 feedbacks translate to an increase in addi-tional global mean radiative forcing of 0.04 $W \cdot m^{-2}$ to 0.19 $W \cdot m^{-2}$ by the end of the 21st century. Under the "worst-case" RCP8.5 scenario, with no climate mitigation, boreal CH_4 emissions are enhanced by 18.05 Tg to 41.69 Tg, due to thawing of inundated areas during the cold season (December to May) and rising temperature, while tropical CH_4 emissions accelerate with a total increment of 48.36 Tg to 87.37 Tg by 2099. Our results suggest that climate mitigation policies must consider mitigation of wetland CH_4 feedbacks to maintain average global warming below 2 °C.

Terrestrial wetlands are among the largest biogenic sources of methane contributing to growing atmospheric CH_4 concentrations (1) and are, in turn, highly sensitive to climate change (2). However, radiative feedbacks from wetland CH_4 emissions were not considered in the Coupled Model Intercomparison Project Phase 5 (CMIP5), and Integrated Assessment Models (IAM) assumed anthropogenic sources to be the only driver responsible for the increase of atmospheric CH_4 burden since the 1750s (3). The role of wetland CH_4 emissions, however, may play an increasingly larger role in future atmospheric growth of methane because of the large stocks of mineral and organic carbon stored under anaerobic conditions in both boreal and tropical regions. Paleoclimatological and contemporary observations of the climate sensitivity of wetland methane emissions suggest the potential for a large feedback (4), but there remains large uncertainty in quantifying the actual range of the response (5, 6).

Increasing air temperature is linked to the thawing of permafrost and to increased rates of soil microbial activity (7), which directly lead to greater CH_4 production in soils due to thaw-induced change in surface wetland areas (8). In the tropics, wetland areal extent is also influenced by precipitation, which affects the area of surface inundation, water table depth, and soil moisture that, in turn, promote methanogenesis. Elevated CO_2 concentrations can increase ecosystem water use efficiency and thus soil moisture, and also increase soil carbon substrate availability for microbial activities (9). Tropical wetlands, for which a decline in inundation was observed in recent decades (10), are already exposed to increasing frequencies in extreme climate events, e.g., heat waves, floods, and droughts, and changes in rainfall distribution (11) and variability in methane emissions (12). Meanwhile, northern high-latitude ecosystems are experiencing a more rapid temperature increase than elsewhere globally and with increased rates of soil respiration (13), yet, locally at least, no response in methane emissions (14). Despite the importance of these feedbacks noted by the Intergovernmental Panel on Climate Change Fifth Assessment Report (IPCC AR5) (15), a comprehensive assessment of long-term global CH_4 feedbacks from changing wetland CH_4 emissions is still lacking.

To address uncertainties related to climate–wetland CH_4 feedbacks, we simulated an ensemble of wetland CH_4 emissions for the 21st century, and then quantified the wetland CH_4 contribution to radiative forcing (RF). Global mean air temperature change was estimated using the reduced complexity carbon cycle and climate model Model for the Assessment of Greenhouse-Gas Induced Climate Change Version 6 (MAGICC6) (16) and a

sustained pulse–response model (17). A state-of-the-art land surface model, Lund–Potsdam–Jena Dynamic Global Vegetation Model (LPJ-DGVM) Wald Schnee und Landscaft version (LPJ-wsl), was used to quantify terrestrial wetland CH_4 emissions, in which permafrost and wetland area distribution and dynamics were estimated prognostically (18). Simulated global CH_4 emissions, calibrated such as to minimize the discrepancy between contemporary global annual CH_4 emissions, were estimated as a function of substrate, soil temperature, and soil moisture (19). Statistically representative estimates of mean and variance of future CH_4 emissions outputs were generated from 112 climate projections originating from 38 climate models of the CMIP5 ensemble (*SI Appendix*, Table S1) covering four Representative Concentration Pathway (RCP) storylines (20).

Materials and Methods

Wetland Definition. Wetlands are defined here as the land area that is either permanently or seasonally saturated, excluding small ponds, lakes, and coastal wetlands. Permanent wetlands comprise three general types: mineral wetlands (swamps and marshes), peatlands (permafrost, bog, fens), and seasonally flooded shallow water (floodplains). The methane-producing area is thus linked to inundation and freeze–thaw dynamics, which change geographically and temporally in response to soil water dynamics.

Model Description. The LPJ-wsl model is a process-based dynamic global vegetation model developed for carbon cycle applications based on development of the LPJ-DGVM (21). LPJ-wsl includes land surface processes, such as water and carbon fluxes, as well as vegetation demography and dynamics that are represented by plant functional types (PFTs) (22). The distribution of PFTs is simulated based on a set of bioclimatic limits and by plant-specific parameters that govern their physiological behavior and their competition for resources. Soil hydrology is modeled using a two-layer bucket model for hydrology and is coupled to an eight-layer freeze–thaw scheme and one-layer snow model to determine permafrost extent and ice content (23, 24) (*SI Appendix, Methods*).

Wetland area and dynamics were simulated following a modified version of the topography-based hydrological model (TOPMODEL) using a prescribed high-resolution topographic index based on a mapping product, hydrological data and maps based on shuttle elevation derivatives at multiple scales (HydroSHEDS) (25). HydroSHEDS was shown to agree most closely with observed wetland area in a comparison with existing global elevation datasets and parameterization schemes (18). Our TOPMODEL approach was optimized by calibrating parameters to match observations from a hybrid wetland area dataset (26) and a regional remote sensing surface inundation dataset (27).

We modeled net wetland CH_4 emissions to the atmosphere restricted to land areas where anaerobic soil conditions create low redox potentials required for methanogenesis. Net CH_4 emissions are estimated daily by combining wetland area (A) within a grid cell (x) with two soil temperature- and moisture-dependent scaling factors ($r_{CH4:C}$ and f_{ecosys}) applied to heterotrophic respiration (R_h),

$$E(x,t) = r_{CH4:C} \cdot f_{ecosys}(x) \cdot A(x,t) \cdot R_h(x,t), \quad [1]$$

where $E(x,t)$ is the net wetland CH_4 flux, $r_{CH4:C}$ is a fixed ratio of soil C to CH_4 emissions, and f_{ecosys} is a modifier that varies the CH_4 emission intensity for different biomes, which is optimized to match average annual emissions from an atmospheric inversion model (28). This approach thus estimates net methane emissions directly, and indirectly accounts for the individual processes of production and consumption of methane, and the various transport processes from the soil to the atmosphere. The comparisons of global and regional net CH_4 emissions between LPJ-wsl and other biogeochemical models are listed in *SI Appendix*, Table S2.

RF Calculations. Two methodologies for calculating RF were used to quantify the climate feedback from additional changes in CH_4 emissions from wetlands. The first method uses the carbon cycle climate model MAGICC6 (16), and the second method uses an emission-driven sustained pulse–response model (17), both relative to a reference year 1765. Because of the challenge to isolate the effect of anthropogenic forcing from wetland forcing in MAGICC6, the simple sustained pulse–response model was used to assess the impact of wetlands on RF by using prescribed anthropogenic sources since 1765 and adding the estimated total wetland emissions from LPJ-wsl. Before 1961, wetland CH_4 emissions were generated, following a uniform distribution, by randomly selecting emissions from 1961 to 1990 to bring the RF value into equilibrium.

In MAGICC6, the lifetime of tropospheric methane is calculated by integrating the effects of hydroxyl radicals (OH) with the temperature-based chemical reaction rates. The observed CH_4 concentration changes over time are more accurately quantified by the net result of variations in emissions of multiple chemical compounds that affect the OH chemical sink, such as ozone, nitrogen oxides, carbon monoxide, and volatile organic compounds. In addition, the net atmospheric lifetime of CH_4 is determined by lifetimes of tropospheric OH, upland soil uptake, and the stratospheric losses. We prescribed the wetland CH_4 concentrations and corresponding anthropogenic CH_4 emissions for each RCP from IPCC AR5 (20).

In contrast, the sustained pulse–response model applies the perturbation lifetime of methane, which is designed to describe the overall long-term RF from CH_4 reactions with OH in the atmosphere (e.g., water vapor in stratosphere), as a constant value of 12.4 y (15). The instantaneous RF from CH_4 contributions at year t since the reference year t', here the year 1765, is given by

$$RF_{CH_4}(t) = \xi_{CH_4} A_{CH_4} \int_0^t \Phi(t') e^{(t'-t)/\tau} dt', \quad [2]$$

where ξ_{CH_4} is a multiplier for CH_4 set to be 1.3; A_{CH_4} is the greenhouse-gas radiative efficiency (1.3×10^{-13} W·m^{-2}·kg^{-1}); and τ_i is the fixed perturbation lifetime for CH_4 (12.4 y). $\Phi(t)$ is a first-order decay function representing the lifetime of an individual net input of CH_4 into the background atmosphere according to IPCC 2013 (15),

$$\Phi(t) = r_0 e^{-\frac{t}{\tau}}, \quad [3]$$

where r_0 is the initial perturbation, and τ is the perturbation lifetime of CH_4. To estimate RF of equal mass of CO_2 in the atmosphere, five CO_2 decay pools with different fractions f_i(26%, 24%, 19%, 14%, and 18%) and adjustment times τ_i (3.4 y, 21 y, 71 y, 421 y, and 10^8 y) are applied to describe the more complicated behavior of CO_2 (17). Thus the total CO_2 RF is given by

$$RF_{CO_2}(t) = \sum_{i=0}^{4} \varepsilon_i A_i f_i \int_0^t \Phi_i(t') e^{(t'-t)/\tau_i} dt'. \quad [4]$$

To quantify the global warming effect of wetland and anthropogenic CH_4 sources, we used a modified metric Sustained Global Warming Potential (SGWP) [unit: kilograms CO_2-equivalents per year (kg CO_2-eq·y^{-1})] (29) to evaluate the total cumulative RF effect from a persistent individual CH_4 source, which was defined as the sum of the time-integrated total RF (unit: watts per square meter), from Eqs. **2** and **4**, over a given time horizon due to a sustained pulse emission of annual CH_4 emission (unit: teragrams) relative to a sustained pulse emission of an equal mass of CO_2 under present-day background conditions. This equation is given by

$$SGWP_{CH_4}(H) = \frac{\sum \int_0^H RF_{CH_4}(t) dt}{\sum \int_0^H RF_{CO_2}(t) dt}, \quad [5]$$

where H represents a certain time horizon. The SGWP for wetland and anthropogenic emissions was calculated with an initial year of 1765.

To quantify the total global warming contribution of wetland CH_4 emissions compared with anthropogenic counterpart, a Wetland Dominance Index (WDI) (unit: percent) was defined using following equation:

$$WDI = \left(\frac{SGWP_{wetland}}{SGWP_{anth}} - 1 \right) \times 100, \quad [6]$$

where $SGWP_{anth}$ represents SGWP caused by anthropogenic activities.

Input Data and Model Experiments. As input to LPJ-wsl, the simulated meteorology, air temperature, total precipitation, and cloud cover from each of the CMIP5 models available from the Earth System Grid Federation was spatially downscaled and bias-corrected to match the spatial resolution (0.5°) and historical period of overlap (1960–1990) from Climatic Research Unit Time Series (CRU TS) Version 3.2.2. We conducted two sets of simulations for each of the climate projections, (*i*) a single spin-up simulation for 1,000 y with randomly selected, detrended 1961–1990 climate, and a constant atmospheric CO_2 concentration of 303 ppm by volume (the average for 1961–1990) and (*ii*) a combined historical and future simulation with time-varying CO_2 and climate data as defined by the corresponding RCP (20).

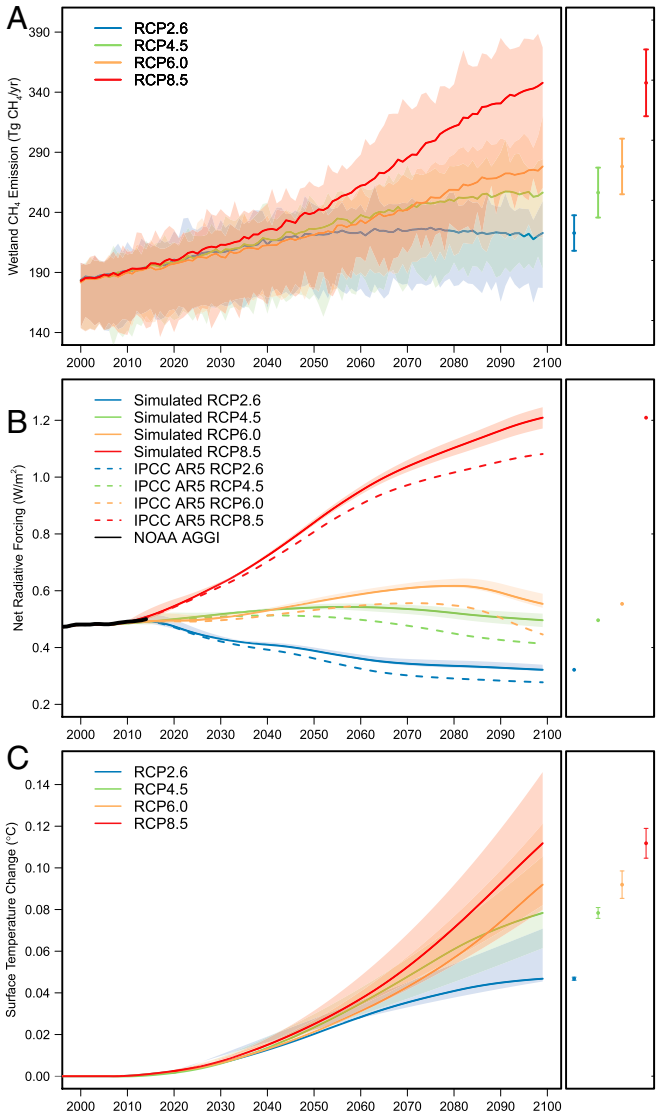


Fig. 1. Simulated future wetland CH_4 emissions, net RF, and net increase in global mean temperature using the simple carbon cycle climate model MAGICC6. Colored lines represent ensemble average estimates from using CMIP5 model outputs, and shaded areas represent the upper and lower range of estimates (*Left*). Mean and one-SD at the end of the 21st century (mean over AD 2099) for each metric are given by the bars (*Right*). (*A*) Simulated wetland CH_4 emissions driven by CMIP5 datasets for four RCPs. (*B*) Net RF from anthropogenic emissions with consideration of wetland CH_4 emissions feedback (solid lines) calculated by MAGICC6 and original projected RCPs without wetland CH_4 feedback (dashed lines) in IPCC AR5 and CMIP5, as well as observed RF (black solid line) based on atmospheric measurement from National Oceanic and Atmospheric Administration (NOAA) Annual Greenhouse Gas Index (AGGI). (*C*) Change in global mean temperature caused by wetland CH_4 feedback from MAGICC6 model.

Uncertainty Analysis. A statistical emulation of LPJ-wsl was parameterized to quantify model structural uncertainty and evaluate how it affected the simulated CH_4 fluxes. We adapted the multiple regression approach from ref. 30 and applied this within a Monte Carlo (MC) analysis to estimate the distribution of CH_4 emissions for each simulation. Parameters in the statistical model were fitted for each RCP. We assumed the parameters of the statistical model followed a normal distribution and used a 2D Latin Hypercube Sampling algorithm to generate 10,000 sets of parameters for each climate projection (*SI Appendix*, Fig. S7). We then conducted MC simulations with Eq. **1**, for a total of 40,000 calculations, to derive the range of CH_4 emissions for each RCP (*SI Appendix*, Fig. S8). These ranges were only applied in MAGICC6 and the simple sustained pulse–response model, to include the impact of model structural uncertainty on RF and SGWP calculations.

Results and Discussion

Mean global annual CH_4 emissions from natural wetlands were projected to increase from 172 Tg $CH_4 \cdot y^{-1}$ (1σ SD, ±12 Tg $CH_4 \cdot y^{-1}$) at present to 221.6 ± 15, 255 ± 20, 272 ± 21, and 338 ± 28 Tg $CH_4 \cdot y^{-1}$ in RCP2.6, RCP4.5, RCP6.0, and RCP8.5, respectively, by 2100 (Fig. 1*A*). In the strong climate mitigation scenario (RCP2.6), which includes the possibility of reaching the policy-relevant 2 °C target, wetland CH_4 emissions peak around the 2050s, with an average of ∼225 Tg $CH_4 \cdot y^{-1}$, and decline thereafter. In contrast, RCP4.5 reveals wetland CH_4 emissions to increase to ∼246 ± 21 Tg $CH_4 \cdot y^{-1}$ before the 2070s and then keep constant, with slightly lower emissions than the RCP6.0 scenario. In the "business-as-usual" scenario, RCP8.5, wetland CH_4 emissions roughly double by the 2090s relative to present-day emissions, with an increasing trend throughout the century. Based on the MAGICC6 approach, we find a 21st century wetland CH_4 RF feedback ranging from 0.04 ± 0.002 $W \cdot m^{-2}$ in RCP2.6, to 0.08 ± 0.003 $W \cdot m^{-2}$ in RCP4.5, to 0.11 ± 0.004 $W \cdot m^{-2}$ in RCP6.0, to 0.19 ± 0.01 $W \cdot m^{-2}$ in RCP8.5 (Fig. 1*B*). These CH_4 RFs estimated by MAGICC6 are equivalent to 0.04 ± 0.001 °C, 0.07 ± 0.004 °C, 0.08 ± 0.006 °C, and 0.12 ± 0.01 °C increases in global mean temperature (Fig. 1*C*) under RCP2.6, RCP4.5, RCP6.0 and RCP8.5, respectively. Compared with the anthropogenic CH_4 emissions, wetlands account for 14.6 to 25.1% of the total projected RF change.

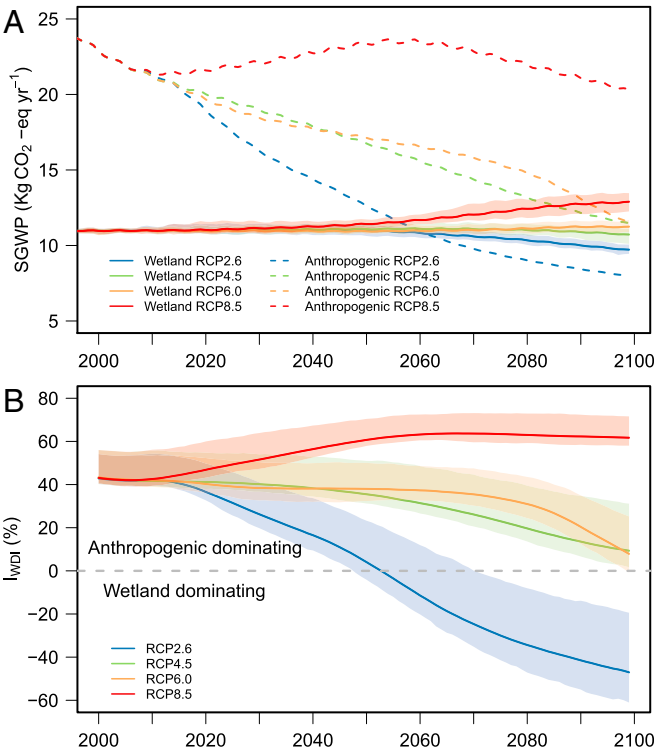


Fig. 2. Evolving pattern of wetland and anthropogenic CH_4 C change over varying time horizon since 1765 using simple sustained pulse–response model. (*A*) Time series of SGWP for wetland and anthropogenic CH_4 emissions. (*B*) Comparison of RF dominance between wetland and anthropogenic emissions. Here RF dominance is defined as a ratio of SGWP from wetlands to SGWP from anthropogenic sources. Shaded areas represent the upper and lower range of wetland estimates. Here the SGWPs from wetland and anthropogenic emissions were calculated as integrated RF of CH_4 since pre-industrial time (1765).

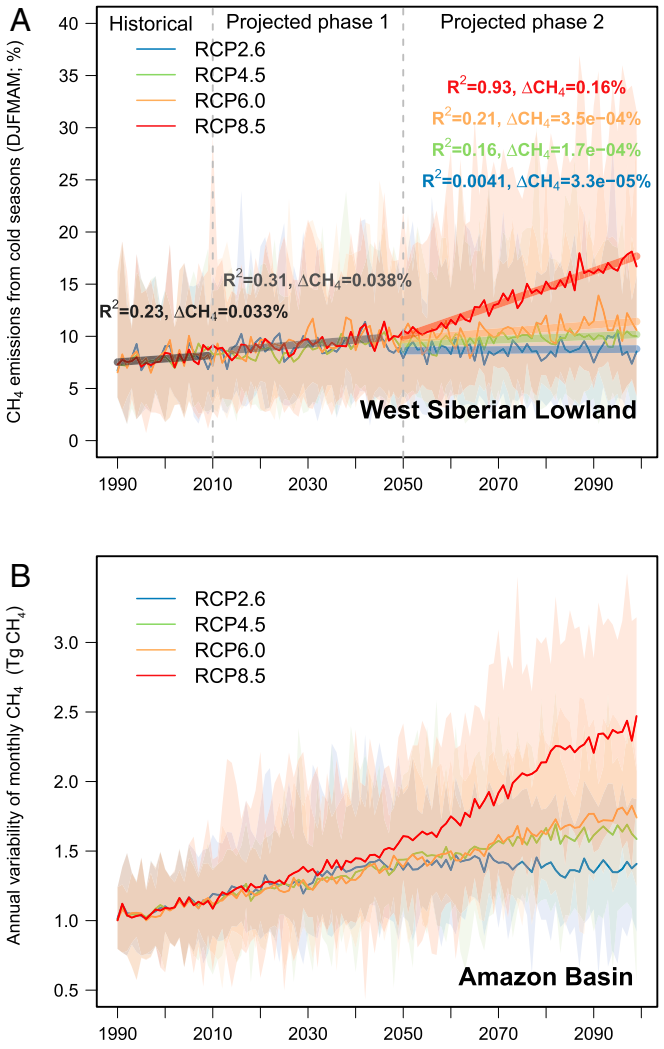


Fig. 3. Regional changes in wetland area extent and CH_4 emissions. (*A*) Contribution of CH_4 emissions from cold seasons (December to May) in boreal wetlands in WSL. Thick lines correspond to linear regression fits of ensemble anomalies. ΔCH_4 represents increasing contribution of CH_4 emission from cold seasons as percentage. (*B*) Annual variability in CH_4 emissions for the Amazon basin, which is defined as SDs of CH_4 fluxes within a year.

The ensemble estimates of SGWP demonstrate the possibility that wetlands overwhelm anthropogenic CH_4 emissions in driving future climate impacts under RCP26 (Fig. 2*B*). The wetland SGWP remains relatively constant at equilibrium state, and then varies with climate scenario (9.7 ± 0.3 kg CO_2-eq·y^{-1}, 10.7 ± 0.3 kg CO_2-eq·y^{-1}, 11.2 ± 0.4 kg CO_2-eq·y^{-1}, and 12.9 ± 0.7 kg CO_2-eq·y^{-1} at the end of the 21st century for RCP26, RCP45, RCP60, and RCP85, respectively) (Fig. 2*A*). The constant SGWP represents an equilibrium state of the global methane budget before 1765, as assumed by IAM whereby chemical sinks balance most of natural emissions. The WDI exhibited large variation driven by RCP scenario, for example, for RCP2.6, natural wetlands clearly play a dominant role by the end of the 21st century, with WDI of $-47 \pm 9\%$. In contrast, the WDI kept a relatively constant value ($55 \pm 8\%$) since the 2050s under RCP8.5, suggesting that climate impact by wetlands is just half of the effect relative to increased anthropogenic emissions. Additionally, the climate feedback parameter, λ, from wetlands CH_4 is $\sim 0.03 \pm 0.001$ W·m^{-2}·K^{-1} under RCP85 (*SI Appendix*, Fig. S6), which falls within the range of previous estimates (2) and is approximately one tenth of the surface albedo feedback from melting snow and ice cover (31).

Changes in 21st century wetland CH_4 emissions are strongly linked to the climate response wetland area extent and seasonality, which showed a diverse response across biomes (*SI Appendix*, Fig. S1). Ignoring potential human modification of wetlands, e.g., peatland drainage, the mean annual maximum global wetland area is expected to be 13% larger ($\sim 0.72 \pm 0.19$ Mkm^2) in the 2090s for RCP8.5 scenario (*SI Appendix*, Fig. S2), whereas earlier studies have assumed no significant change in wetland area (32). Regionally, reduced precipitation causes a small decrease ($\sim 0.06 \pm 0.01$ Mkm^2 for RCP85) in tropical wetland area, whereas thawing of the near-surface permafrost stimulates a large increase ($\sim 0.58 \pm 0.15$ M·km^2 for RCP85) in boreal wetland area. However, despite decreasing tropical wetland extent and increased frequency of tropical drought, tropical wetlands remain the world's largest

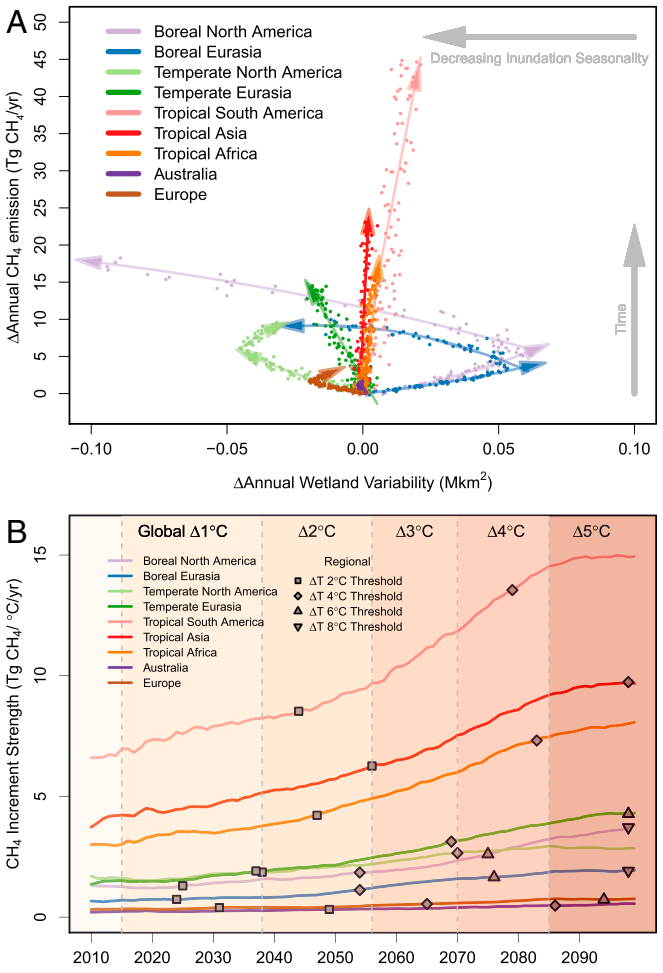


Fig. 4. Role of regional wetlands in changing wetland status and CH_4 emissions. (*A*) Scatterplot shows relationship between ensemble anomalies of annual wetland variability and anomalies of annual CH_4 emissions relative to 1960–1990 average levels for regional wetlands under RCP8.5. The linear least square regression fits represent the evolving trajectories of CH_4 emissions with increasing CH_4 emissions. The horizontal arrow represents the direction of increasing wetland CH_4 emissions with shifting patterns of inundation seasonality. The vertical arrow represents the evolving directions of both CH_4 emissions and inundation seasonality with time. (*B*) Increment of CH_4 emissions with rising temperature for regional wetlands. Background colors represent increases of global temperature from ensemble estimate of CMIP5 models under RCP8.5. Dots indicate regional increase of temperature at certain time. Details of calculation are provided in *SI Appendix, Methods*.

natural source responsible for ~53.2 ± 0.7% by the end of the 21st century in RCP8.5. The annual contribution of boreal wetlands increases by ~3.6 ± 0.5% from the present to the end of the 21st century, indicating higher sensitivity to climate change-driven CH_4 emissions in boreal regions because of thawing permafrost.

The increase in methane-producing wetlands in boreal regions was due primarily to increased near-surface soil moisture following permafrost thaw. More than half of global wetland area is positively correlated with air temperature while ~40% is negatively correlated (*SI Appendix*, Fig. S3). For instance, the West Siberian Lowland (WSL), one of the largest boreal wetlands, comprising ~12.9% of the global peatland area, exhibits an increase in CH_4 emissions during the transition from winter to spring, i.e., December to May (*SI Appendix*, Fig. S4). This originates from an increase in the thaw period and from higher heterotrophic respiration induced by higher soil temperatures. Projected thawing of permafrost and associated wetland expansion will largely affect CH_4 emissions from the taiga forest region in the WSL. From around the mid-2040s, a strong linear increase ($R^2 = 0.93$, $P < 0.01$) of CH_4 emissions with time, at a rate of 0.16% per year from winter to spring seasons, will occur under RCP8.5, despite environmental conditions changing more slowly in the WSL ($R^2 < 0.21$, $P > 0.01$) under all scenarios (Fig. 3*A*).

Long-term simulated tropical CH_4 emission changes are mainly associated with a shift in precipitation patterns. The partial correlation between global CH_4 emissions and climatic variables shows that spatial variation of CH_4 emissions is associated mainly with precipitation, and that this is especially important in tropical regions where the annual cycle of wet to dry seasons varies considerably. Consistent with an observed increase in the dry season in Amazonia since 1979 (11), our ensemble estimates predict a slightly negative trend in the basin-wide annual areal maximum of Amazonian wetlands by ~4% by the 2090s under RCP8.5. Despite there being no significant change in the proportion of CH_4 emissions from dry seasons across all RCP scenarios, we did find a steady increase in annual variability of CH_4 emissions (Fig. 3*B*).

We found a statistically significant relationship between seasonal wetland area variability and the increase in annual CH_4 emissions, despite diverse mechanisms driving large-scale CH_4 emission changes among wetlands (Fig. 4*A*). In addition, we show that seasonality of wetland area is an indicator for monitoring the long-term dynamics of CH_4 emissions at continental scale. Altered patterns in the trend of wetland variability coincide with the onset of a strong linear increase in CH_4 emissions in boreal wetlands, which suggests that CH_4 emissions are largely increased during cold seasons (December to February, March to May) afterward (*SI Appendix*, Fig. S5). The net growth rate of CH_4 emissions from the summer to autumn seasons is larger than that from the winter to spring seasons after the 2040s. In addition, the growth rates measured by regression lines among all regions characterize the strength of emitting CH_4 among major regions, where tropical wetlands show higher contributions than the other regions.

Our CH_4 RF estimates are subject to considerable uncertainties associated with estimation of natural sources and the resulting climate feedback. The representation of processes in LPJ-wsl assumes no effect of shifting spatial pattern of vascular plants on CH_4 transport from soil into atmosphere, which could lead to an underestimation of CH_4 emissions. Furthermore, microbial community composition might play an important role in driving CH_4 fluxes, but the biogeographical distribution of methanogen communities and their metabolic processes at ecosystem-scale are poorly understood due to the lack of observational data. In addition, uncertainties in RF estimates are also associated with the parameter values of the CH_4 lifetime and variations of global chemical CH_4 sinks, e.g., OH concentrations. To better understand the evolution of atmospheric CH_4 concentrations in the future, comprehensive in situ and remote sensing monitoring of CH_4 emissions and changes in wetland area are required.

The potential sensitivity of wetland CH_4 emissions to rising temperature highlights the need for limiting global warming below the 2 °C target. Climate-driven CH_4 emission feedbacks were positive for each wetland region (Fig. 4*B*), with large variability related to the different sensitivities of methanogenesis, freeze–thaw dynamics, and surface inundation. The timing of feedbacks was also variable, with increases in tropical wetlands emissions appearing to have a fairly abrupt response once global mean temperature approached 2 °C warming, whereas boreal wetlands, especially boreal North America, had more gradual increases in emissions due to expanding wetland area (33). Taking into account these additional changes in RF caused by increasing wetland CH_4 emissions emphasizes the need to consider wetland CH_4 feedbacks in IAM and to develop comprehensive greenhouse gas mitigation strategies. In addition, policy-relevant temperature targets must continue to incorporate assessments of feedbacks from terrestrial and oceanic systems for both CO_2 and non-CO_2 gases, like methane and nitrous oxide. With atmospheric methane concentrations now tracking the more fossil fuel-intensive scenarios (34), further insight into the climate sensitivity of methane sources and their chemical sinks remains of high importance.

ACKNOWLEDGMENTS. We thank Benjamin D. Stocker, Thomas Peter, Joeri Rogelj, and Leonardo Calle for constructive comments on the manuscript. We also thank Wolfgang Lucht and the anonymous reviewers for their detailed comments on the manuscript. We acknowledge the World Climate Research Programme's Working Group on Coupled Modeling, which is responsible for CMIP, and we thank the climate modeling groups for producing and making available their model outputs. Computational efforts were performed on the Hyalite High-Performance Computing System, operated and supported by Montana State University Information Technology Research Cyberinfrastructure. This study was funded by the Competence Center Environment and Sustainability (CCES) Project Modeling and Experiments on Land-Surface Interactions with Atmospheric Chemistry and Climate Phase 2 (MAIOLICA2) 42-01, Chinese Academy of Sciences (CAS) Project Big Earth Data Engineering, and the National Natural Science Foundation of China (Grants T411391001 and 91425303). This paper does not reflect the official views or policies of the United States Government or any agency thereof, including the Department of Energy.

1. Tian H, et al. (2016) The terrestrial biosphere as a net source of greenhouse gases to the atmosphere. *Nature* 531:225–228.
2. Arneth A, et al. (2010) Terrestrial biogeochemical feedbacks in the climate system. *Nat Geosci* 3:525–532.
3. Taylor KE, Stouffer RJ, Meehl GA (2011) An overview of CMIP5 and the experiment design. *Bull Am Meteorol Soc* 93:485–498.
4. Hopcroft PO, Valdes PJ, O'Connor FM, Kaplan JO, Beerling DJ (2017) Understanding the glacial methane cycle. *Nat Commun* 8:14383.
5. Schaefer H, et al. (2016) A 21st-century shift from fossil-fuel to biogenic methane emissions indicated by $^{13}CH_4$. *Science* 352:80–84.
6. Nisbet EG, et al. (2016) Rising atmospheric methane: 2007–2014 growth and isotopic shift. *Global Biogeochem Cycles* 30:1356–1370.
7. Yvon-Durocher G, et al. (2014) Methane fluxes show consistent temperature dependence across microbial to ecosystem scales. *Nature* 507:488–491.
8. Cooper MDA, et al. (2017) Limited contribution of permafrost carbon to methane release from thawing peatlands. *Nat Clim Change* 7:507–511.
9. van Groenigen KJ, Osenberg CW, Hungate BA (2011) Increased soil emissions of potent greenhouse gases under increased atmospheric CO_2. *Nature* 475:214–216.
10. Prigent C, et al. (2012) Changes in land surface water dynamics since the 1990s and relation to population pressure. *Geophys Res Lett* 39:L08403.
11. Fu R, et al. (2013) Increased dry-season length over southern Amazonia in recent decades and its implication for future climate projection. *Proc Natl Acad Sci USA* 110:18110–18115.
12. Pandey S, et al. (2017) Enhanced methane emissions from tropical wetlands during the 2011 La Niña. *Sci Rep* 7:45759.
13. Commane R, et al. (2017) Carbon dioxide sources from Alaska driven by increasing early winter respiration from Arctic tundra. *Proc Natl Acad Sci USA* 114:5361–5366.
14. Sweeney C, et al. (2016) No significant increase in long-term CH_4 emissions on North Slope of Alaska despite significant increase in air temperature. *Geophys Res Lett* 43:6604–6611.
15. Intergovernmental Panel on Climate Change (2013) *Climate Change 2013: The Physical Science Basis. Contribution of Working Group I to the Fifth Assessment*

Report of the Intergovernmental Panel on Climate Change (Cambridge Univ Press, Cambridge, UK).
16. Meinshausen M, Raper SCB, Wigley TML (2011) Emulating coupled atmosphere-ocean and carbon cycle models with a simpler model, MAGICC6 – Part 1: Model description and calibration. *Atmos Chem Phys* 11:1417–1456.
17. Frolking S, Roulet N, Fuglestvedt J (2006) How northern peatlands influence the Earth's radiative budget: Sustained methane emission versus sustained carbon sequestration. *J Geophys Res Biogeosci* 111:G01008.
18. Zhang Z, Zimmermann NE, Kaplan JO, Poulter B (2016) Modeling spatiotemporal dynamics of global wetlands: Comprehensive evaluation of a new sub-grid TOPMODEL parameterization and uncertainties. *Biogeosciences* 13:1387–1408.
19. Hodson EL, Poulter B, Zimmermann NE, Prigent C, Kaplan JO (2011) The El Niño–Southern Oscillation and wetland methane interannual variability. *Geophys Res Lett* 38:L08810.
20. Meinshausen M, et al. (2011) The RCP greenhouse gas concentrations and their extensions from 1765 to 2300. *Clim Change* 109:213–241.
21. Sitch S, et al. (2003) Evaluation of ecosystem dynamics, plant geography and terrestrial carbon cycling in the LPJ dynamic global vegetation model. *Global Change Biol* 9:161–185.
22. Poulter B, et al. (2011) Plant functional type mapping for earth system models. *Geosci Model Dev* 4:993–1010.
23. Gerten D, Schaphoff S, Haberlandt U, Lucht W, Sitch S (2004) Terrestrial vegetation and water balance—Hydrological evaluation of a dynamic global vegetation model. *J Hydrol (Amst)* 286:249–270.
24. Wania R, Ross I, Prentice IC (2009) Integrating peatlands and permafrost into a dynamic global vegetation model: 1. Evaluation and sensitivity of physical land surface processes. *Global Biogeochem Cycles* 23:GB3014.
25. Marthews TR, Dadson SJ, Lehner B, Abele S, Gedney N (2015) High-resolution global topographic index values for use in large-scale hydrological modelling. *Hydrol Earth Syst Sci* 19:91–104.
26. Poulter B, et al. (2016) Global wetland contribution to increasing atmospheric methane concentrations (2000–2012). *Environ Res Lett*, in press.
27. Hess L, et al. (2015) Wetlands of the lowland Amazon basin: Extent, vegetative cover, and dual-season inundated area as mapped with JERS-1 synthetic aperture radar. *Wetlands* 35:745–756.
28. Spahni R, et al. (2011) Constraining global methane emissions and uptake by ecosystems. *Biogeosciences* 8:1643–1665.
29. Neubauer S, Megonigal JP (2015) Moving beyond global warming potentials to quantify the climatic role of ecosystems. *Ecosystems (N Y)* 18:1000–1013.
30. Piao S, et al. (2013) Evaluation of terrestrial carbon cycle models for their response to climate variability and to CO_2 trends. *Global Change Biol* 19:2117–2132.
31. Soden BJ, Held IM (2006) An assessment of climate feedbacks in coupled ocean–atmosphere models. *J Clim* 19:3354–3360.
32. Stocker BD, et al. (2013) Multiple greenhouse-gas feedbacks from the land biosphere under future climate change scenarios. *Nat Clim Change* 3:666–672.
33. Serreze M, Francis J (2006) The Arctic amplification debate. *Clim Change* 76:241–264.
34. Saunois M, Jackson RB, Bousquet P, Poulter B, Canadell JG (2016) The growing role of methane in anthropogenic climate change. *Environ Res Lett* 11:120207.

SI Appendix

Supporting Methods

1. LPJ-wsl Description

The parameters of $r_{CH4:C}$ and f_{ecosys} in LPJ-wsl methane model used in this study are calibrated together as a scaling ratio F(x) to a global CH_4 fluxes from an inversion model (1) by fitting a function of two weighted-regional scaling factors, one representing tropical (-30°S-30°N, F_T) and the other representing boreal (45°N-90°N, F_B) wetland climate:

$$F(x) = r_{CH4:C} \cdot f_{ecosys}(x) = \sigma(x) \cdot F_T + (1 - \sigma(x)) \cdot F_B \quad (1)$$

where $\sigma(x)$ represents the CH_4-emitting capacity function. By using this approach, the model is capable to account for broad ecosystem difference in CH_4-emitting capacity among wetland ecosystem types. The weighting of wetland land type is prognostically defined based on surface temperature using equations below:

$$\sigma(x) = \exp(T(x) - T_{max})/8 \quad (2)$$

where T(x) represents mean surface temperature, and T_{max}=303.35°K. The mean surface temperature map is using annual average of 1960-1990 from CRU TS 3.2.2. After applying a non-linear least fitting with Gauss-Newton method, we derived the F_T and F_B with value of 0.0418 and 0.0163 respectively.

The permafrost module in LPJ-wsl is based on LPJ-WHyMe v.1.3.1 (2) freeze/thaw cycle and dynamics snow module with an updated soil parameterizations (3). Soil texture is based on the Harmonized World Soil Database using the Cosby equation (4) to calculate water-holding capacity for the upper and lower layers. The response of ecosystem respiration rate to air temperature is based on empirical relationships, which incorporate damping of Q_{10} response due to temperature acclimation (5). This version considers the reduction of water infiltration in frozen soil, which is represented by scaling the potential infiltration with the reduction of liquid water holding capacity within the upper soil layer (0-20 cm) by presence of ice in the soil (6), which leads to an increase of surface runoff during early spring and thus affect CH_4 emissions through influencing the plant water stress function and water availability for litter degradation .

2. Anthropogenic emission and concentration datasets

The anthropogenic CH_4 emissions for MAGICC6 simulations were from RCP Database v2.0 (http://tntcat.iiasa.ac.at:8787/RcpDb, last accessed July 12th, 2017), in which harmonized and consolidated greenhouse gases data are projected for 4 RCPs. The CH_4 concentration datasets for RCPs applied for the simple sustained-pulse model were from prescribed IPCC AR5 trajectories, which were simulated by MAGICC6 based on combining a suite of atmospheric concentration observations and emissions estimates for historical period and the

harmonized emission projected by four different Integrated Assessment Models for 2005-2100 (7). See Table S3 for the emissions by model and Dataset S1 for ensemble mean estimates of wetland CH_4 emissions and wetland areas.

3. Uncertainty Analysis

A Monte Carlo analysis with one box model were applied to investigate the uncertainties of the CH_4 estimates from LPJ-wsl. We adapted a multiple regression approach from Piao*, et al.* (8) to empirically estimate the response of CH_4 emissions to climate variability (interannual Mean Annual Temperature (MAT) and annual precipitation) over the future RCPs:

$$y = \gamma^{int} x_T + \delta^{int} x_P + \varepsilon \quad (3)$$

where y is the detrended anomaly of CH_4 emissions from the LPJ-wsl simulation for each RCPs. The variables x_T is the detrended MAT anomaly, and x_P is the detrended annual precipitation anomaly. The fitted regression coefficients γ^{int} and δ^{int} define the apparent CH_4 emission sensitivity to interannual variations in temperature and precipitation, and the ε the residual error. The detrending function from *TTR* R package (http://CRAN.R-project.org/package=TTR) was used to detrend the anomalies of temperature, precipitation, and CH_4 emissions. The regression coefficients are calculated using maximum likelihood estimates (MLE). Please note that here for simplicity, we assume γ^{int} and δ^{int} is the dominant effect of climate variations on CH_4 emissions and temperature and precipitation are independent, although actually they might covary over time. Figure R1 clearly show the different distribution of derived CH_4 sensitivity of LPJ-wsl to climate variations, where CH_4 emissions is more sensitive to temperature change among RCPs while it doesn't show significant difference in precipitation pattern among RCPs. Then we assume these two parameters following normal distributions, and used a Latin Hypercube sampling (LHS) algorithm to develop 10,000 sets of parameters for each RCP. We then conducted Monte Carlo (MC) simulations with equation (1) for a total of 40,000 calculations. Based on these MC ensemble simulations, we quantitatively estimate the potential uncertainties of CH_4 emission that include the uncertainty from CMIP5 forcings, as well as the uncertainty from model structure.

4. Partial Correlation

We performed two sets of partial correlation analysis: (1) ensemble estimated wetland area from LPJ-wsl and ensemble of precipitation, and temperature from CMIP5 outputs; (2) ensemble estimated CH_4 emission from LPJ-wsl and precipitation and temperature from CMIP5. In Fig S3 and Fig. S4 the resulting significant ($p < 0.01$) correlation are shown.

5. Climate feedback calculation

We adopt the linear assumption of climate feedback and use equation to calculate climate feedback parameter λ :

$$F - N = \lambda \Delta T \quad (4)$$

where F is net forcing strength, N represents net heat flux uptake by ocean, ΔT represents the climate states. All the variables above are derived from MAGICC6 simulations to calculate the parameter λ for each RCP. The wetland CH_4 feedback is calculated by the parameter derived from scenarios with wetland CH_4 emission subtracting that without wetland CH_4 emissions. Fig. S6 shows the time evolution of wetland CH_4 feedback for each RCP.

6. Calculation of CH_4 emissions response to rising temperature

In Fig. 4b, increments of wetland CH_4 emissions with rising temperature for regional wetlands (defined in Fig. S1) are calculated as the ratio of annual total CH_4 emission increment (delta Tg/yr) to area-weighted annual mean temperature increment (delta °C) for each regional wetland. The ratios of wetland CH_4 emissions response to changing temperature were estimated continuously using a 10-year moving window from 2000 to 2100.

Supporting Information:

Table S1. Details of the WCRP CMIP5 global climate models used in this study. Check marks indicate which scenarios were used.

Model	Country	Institute	RCP2.6	RCP4.5	RCP6.0	RCP8.5
ACCESS1.0	Australia	Commonwealth Scientific and Industrial Research Organisation		✓		✓
ACCESS1.3	Australia	Commonwealth Scientific and Industrial Research Organisation		✓		✓
BCC_CSM1.1	China	Beijing Climate Center, China Meteorological Administration	✓	✓	✓	✓
BCC_CSM1.1-m	China	Beijing Climate Center, China Meteorological Administration	✓	✓	✓	✓
BNU-ESM	China	College of Global Change and Earth System Science, Beijing Normal University	✓	✓		✓
CanESM2	Canada	Canadian Centre for Climate Modelling and Analysis	✓	✓		✓
CCSM4	United States	National Center for Atmospheric Research	✓		✓	✓
CESM1(BGC)	United States	National Science Foundation, U. S. Department of Energy, and National Center for Atmospheric Research		✓		✓
CESM1(CAM5)	United States	National Science Foundation, U. S. Department of Energy, and National Center for Atmospheric Research	✓	✓	✓	✓
CMCC-CM	Italy	Centro Euro-Mediterraneo per I Cambiamenti Climatici		✓		✓
CMCC-CMS	Italy	Centro Euro-Mediterraneo per I Cambiamenti Climatici		✓		✓

CMCC-CESM	Italy	Centro Euro-Mediterraneo per I Cambiamenti Climatici				✓
CNRM-CM5	France	Centre National de Recherches Météorologiques	✓	✓		✓
CSIRO Mk3.6.0	Australia	Commonwealth Scientific and Industrial Research Organisation	✓	✓	✓	✓
FGOALS-g2	China	LASG, Institute of Atmospheric Physics, Chinese Academy of Sciences	✓	✓		
FIO-ESM	China	The First Institute of Oceanography	✓	✓	✓	✓
GFDL CM3	United States	NOAA/Geophysical Fluid Dynamics Laboratory	✓		✓	✓
GISS-E2-H	United States	NASA Goddard Institute for Space Studies	✓	✓	✓	✓
GISS-E2-H-CC	United States	NASA Goddard Institute for Space Studies		✓		
GISS-E2-R	United States	NASA Goddard Institute for Space Studies	✓	✓	✓	✓
GISS-E2-R-CC	United States	NASA Goddard Institute for Space Studies		✓		
HadGEM2-AO	United Kingdom	Met Office Hadley Centre	✓	✓	✓	✓
HadGEM2-CC	United Kingdom	Met Office Hadley Centre		✓		✓
HadGEM2-ES	United Kingdom	Met Office Hadley Centre	✓	✓		
INM CM4	Russia	Institute of Numerical Mathematics		✓		✓
IPSL-CM5A-LR	France	L'Institut Pierre-Simon Laplace	✓	✓	✓	✓
IPSL-CM5A-MR	France	L'Institut Pierre-Simon Laplace	✓	✓	✓	✓
IPSL-CM5B-LR	France	L'Institut Pierre-Simon Laplace		✓		✓

MIROC-ESM	Japan	Atmosphere and Ocean Research Institute (AORI, University of Tokyo), National Institute for Environmental Studies (NIES), and JAMESTEC	✓	✓	✓	✓
MIROC-ESM-CHEM	Japan	AORI (University of Tokyo), NIES, and JAMESTEC	✓	✓	✓	✓
MIROC5	Japan	AORI (University of Tokyo), NIES, and JAMESTEC	✓	✓	✓	✓
MPI-ESM-LR	Germany	Max Planck Institute for Meteorology	✓	✓		✓
MPI-ESM-MR	Germany	Max Planck Institute for Meteorology	✓	✓		✓
MRI-CGCM3	Japan	Meteorological Research Institute	✓	✓	✓	✓
NorESM1-M	Norway	Norwegian Climate Centre	✓		✓	✓
NorESM1-ME	Norway	Norwegian Climate Centre	✓		✓	✓

100

101

Table S2. List of global wetland methane estimates (unit: Tg CH_4/yr) from our ensemble estimates using CMIP5 models and other studies over the period 1980-2000.

Estimates	Global	Regions			Hotspot			
		Tropics (20N-30S)	Temperate (20-50N, 30S-50S)	Northern (>50N)	Amazon	WSL	Hudson Bay	Alaska
Bottom-up								
LPJ-wsl	172.1±10.7	125.7±3.0	22.9±0.95	23.4±0.76	30.9±0.8	3.5±0.1	4.2±0.21	1.7±0.2
WETCHIMP experiment(9)[a]	190±39	126±31					5.4±3.2	
Zhu2015(10)	209-245			38.1-55.4				
Chen2015(11)				35*			3.11±0.45	
Zhu2014(12)				34-58*			3.1± 0.5	
Meng2012(13)	256	201		12				
Ringeval2012(6)	193.8	102	51	40.8				
Riley2011(14)	270	160	50	70*				
Glagolev2011(15)						3.91±1.3		

Wania2010(2)				57.2*			
Melack2004(16)					22		
Zhuang2004(17)				57.3*			
Walter2000(18)	260	186	26	48			
Cao1996(19)	92	51.4	17.2	23.3			
Christensen1996(20)				20±13			
Top-down							
Chang2014(21)							2.1±0.5
Miller2014(22)						1.8±0.24	
Pickett-Heaps2011(23)						2.3±0.3	
Bousquet2011(24)	151±10	91±11					
Bloom2010(25)	165±50	91±28				4.9±1.4	
Bousquet2006(26)	159.5	103	25	31.5			
Chen2006(27)				34±13			
Fletcher2004(28)	231±46						

Wang et al., 2004(29)	176±10
Houweling et al., 2000(30)	163±16

104

105

Table S3. List of LPJ-wsl simulated wetland CH_4 emissions for future RCPs by CMIP5 model.

Model	CH_4 emissions in 2050 (Tg CH_4/yr)				CH_4 emissions in 2099 (Tg CH_4/yr)			
	RCP2.6	RCP4.5	RCP6.0	RCP8.5	RCP2.6	RCP4.5	RCP6.0	RCP8.5
ACCESS1.0		223.3		254.2		258.5		373.7
ACCESS1.3		254.4		242.4		261.4		352.7
BCC_CSM1.1	222.2	221.8	223.8	247.5	221.3	245.2	273.6	364.5
BCC_CSM1.1-m	222.5	223.6	219.1	233.9	225.6	251.8	273.6	338.6
BNU-ESM	226.5	239.0		248.9	233.4	274.9		375.5
CanESM2	214.7	221.9		238.2	218.4	241.8		324.1
CCSM4	222.3		224.5	243.5	231.9		280.5	357.9
CESM1 (BGC)		235.0		234.4		253.5		355.2
CESM1 (CAM5)	237.7	240.3	231.1	265.2	249.2	283.7	307.6	371.4
CMCC-CM		235.5		244.3		266.1		373.8
CMCC-CMS		221.9		239.5		271.7		368.6
CMCC-CESM				247.3				364.5
CNRM-CM5	225.3	236.6		237.8	231.8	269.4		358.7
CSIRO Mk3.6.0	227.3	232.7	197.9	231.4	220.7	222.2	258.5	299.3

FGOALS-g2	229.3	229.1			227.5	279.5		
FIO-ESM	214.6	223.9	222.8	238.9	223.1	259.5	273.3	337.4
GFDL CM3	236.3		229.6	257.0	229.7		293.8	364.3
GISS-E2-H	217.89	226.4	228.2	239.8	221.9	271.3	288.6	**334.8**
GISS-E2-H-CC		230.5				257.5		
GISS-E2-R	208.9	225.1	229.0	238.2	228.0	252.9	275.3	334.5
GISS-E2-R-CC		226.3				260.2		
HadGEM2-AO	224.8	238.0	221.9	238.9	218.6	272.2	290.9	350.3
HadGEM2-CC		242.7		253.9		254.6		365.1
HadGEM2-ES	225.0	242.4			226.3	284.1		
INM CM4		238.3		263.4		257.6		367.1
IPSL-CM5A-LR	172.5	178.8	187.3	190.5	181.4	217.0	219.1	301.1
IPSL-CM5A-MR	177.1	180.1	177.9	191.7	177.1	214.1	236.0	296.7
IPSL-CM5B-LR		167.5		177.9		193.0		260.4
MIROC-ESM	231.2	245.3	227.3	265.8	226.0	271.0	319.7	369.9
MIROC-ESM-CHEM	246.6	234.0	249.8	255.7	239.0	269.1	291.1	373.7
MIROC5	230.0	237.3	222.5	243.7	222.2	269.1	278.5	377.2

MPI-ESM-LR	222.3	226.4		235.5	219.9	253.0		329.7
MPI-ESM-MR	213.0	222.0		233.1	226.9	262.5		364.5
MRI-CGCM3	224.6	216.9	219.9	229.4	224.1	251.4	285.8	331.9
NorESM1-M	220.5		229.6	240.1	223.9		279.9	334.9
NorESM1-ME	231.7		229.3	240.2	221.9		281.3	356.1
Mean±Sd(1σ)	222.0±16.1	226.4±19.0	220.6±16.9	238.5±19.8	222.8±14.8	256.4±20.8	278.2±23.1	347.8±27.8

107

108

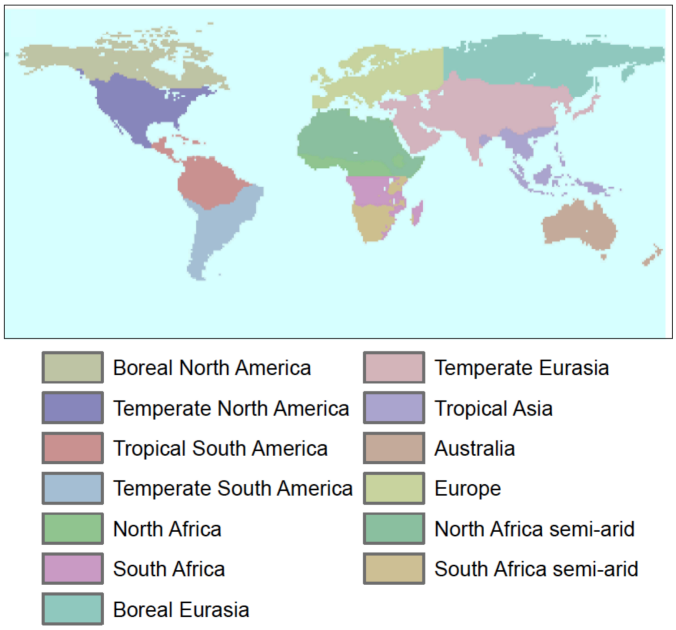


Figure S1. Map of regions used to partition the globe into boreal, tempe
tropical and arid/semi-arid biomes. North Africa and South Africa tog
considered as Tropical Africa regions in Fig. 4.

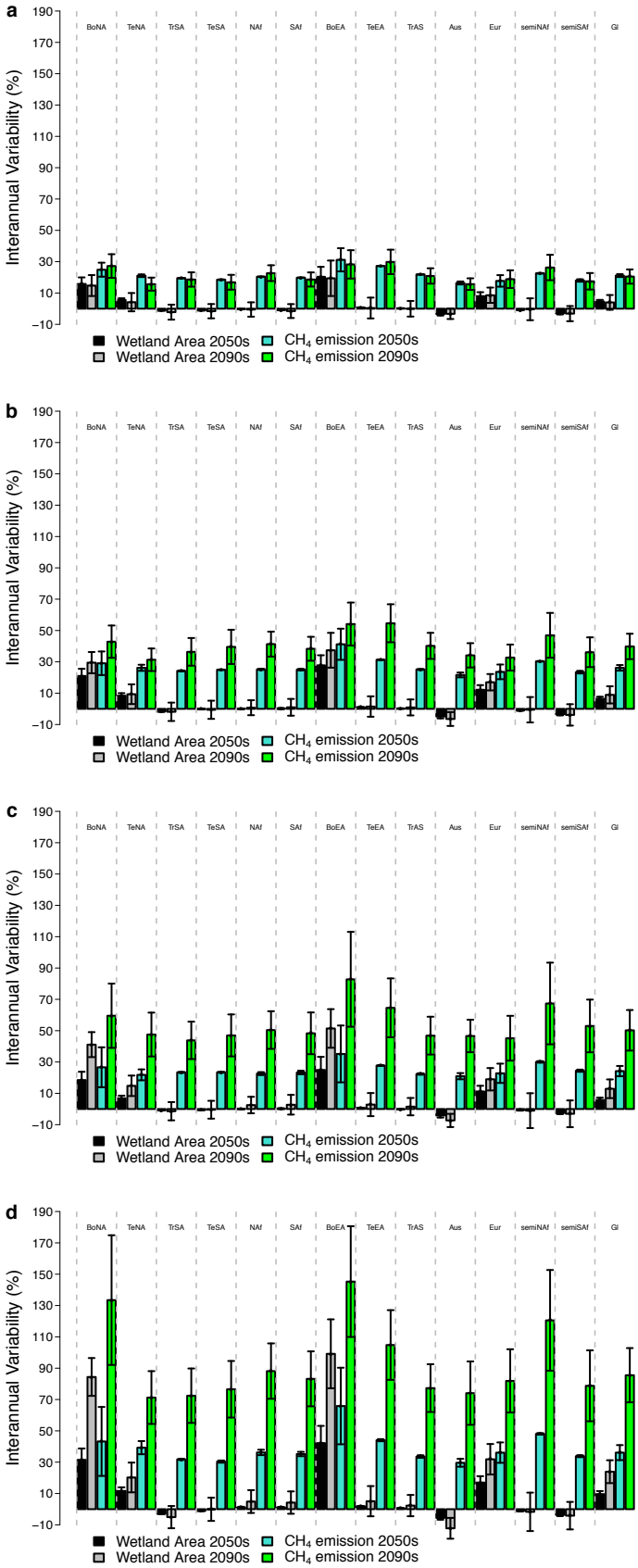
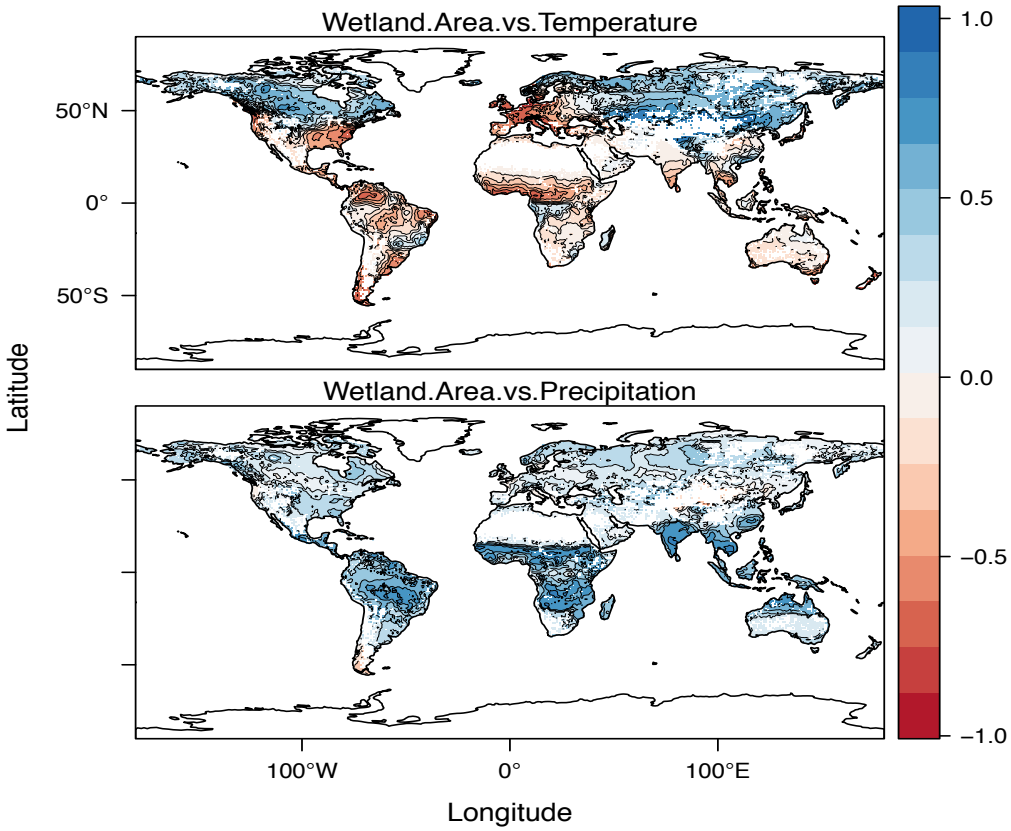


Figure S2. Interannual variability in wetland area and CH_4 emissions (error bars represent 1σ standard deviation of all model estimates) in the 2050s and 2090s

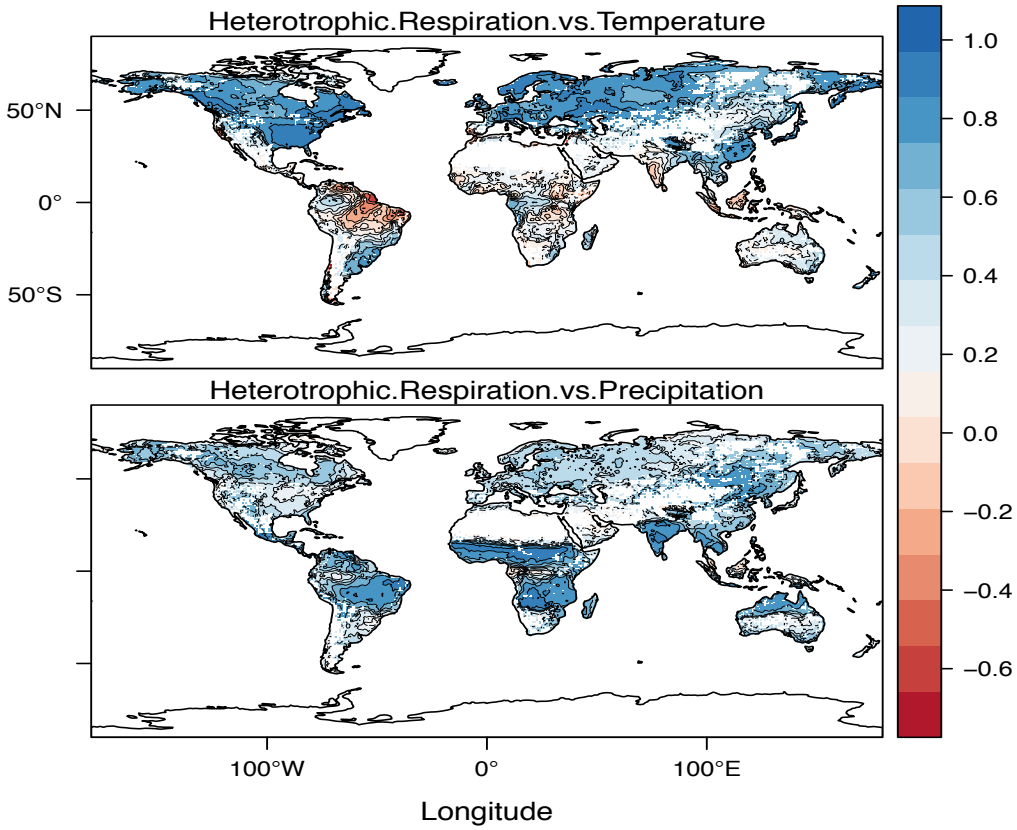
relative to historical levels (average of 1960-1990) for 13 regions and the global average (BoNA: Boreal North America; TeNA: Temperate North America; TrSA: Tropical South America; TeSA: Temperate South America; NAf: North Africa; SAf: South Africa; BoEA: Boreal Eurasia; TeEA: Temperate Eurasia; TrAS: Tropical Asia; Aus: Australia; Eur: Europe; semiNAf: semi-arid North Africa; semiSAf: semi-arid South Africa; Gl: Global) under **a.** RCP2.6, **b.** RCP4.5, **c.** RCP6.0, and **d.** RCP8.5 scenario.



125

126 **Figure S3.** Regional partial correlations between wetland area from LPJ-wsl and
127 either temperature (top) or precipitation (bottom). This analysis has been
128 carried out for 2.5° by 2.5° moving windows. Therefore, for each 0.5° pixel, the
129 surrounding 5x5=25 pixels have been used. Shown are significant correlations
130 ($p<0.01$) of which the correlation coefficient is higher/lower than ±0.2.

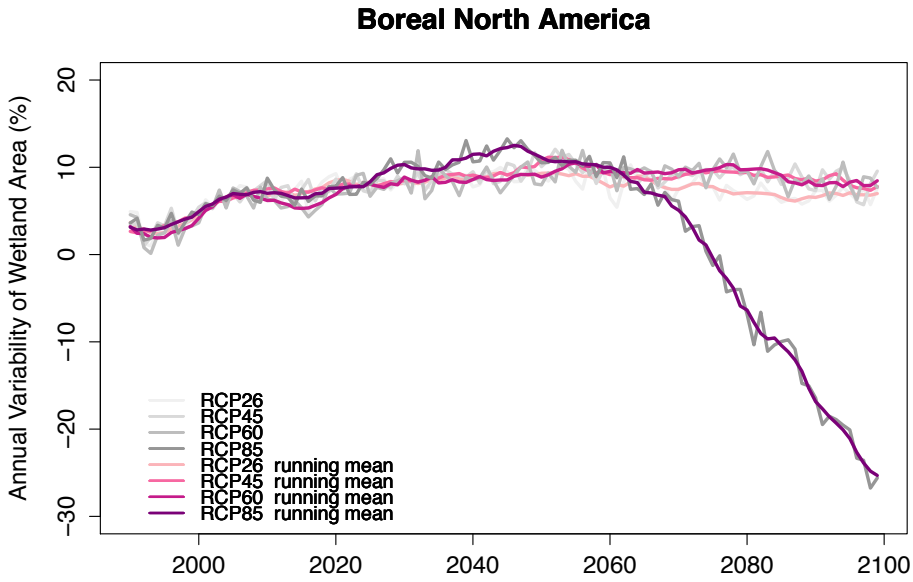
131



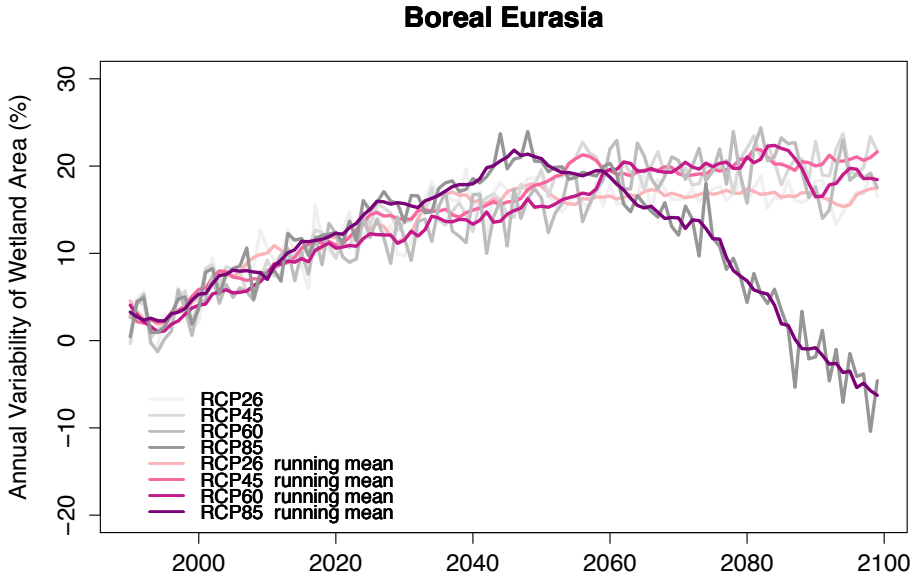
132

133 **Figure S4.** Regional partial correlations between heterotrophic respiration from
134 LPJ-wsl and either temperature (top) or precipitation (bottom). This analysis has
135 been carried out for 2.5° by 2.5° moving windows surrounding each 0.5° pixel.
136 Shown are significant correlations ($p<0.01$) of which the correlation coefficient is
137 higher/lower than ±0.2.

138

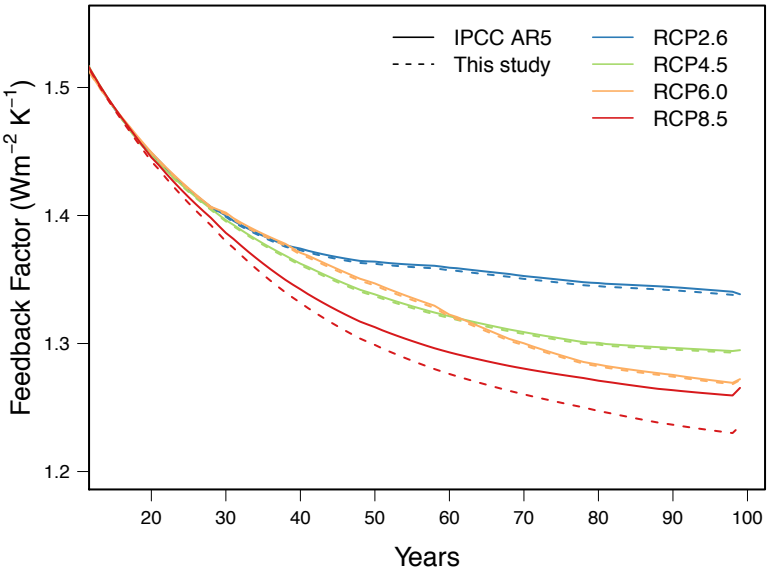


139



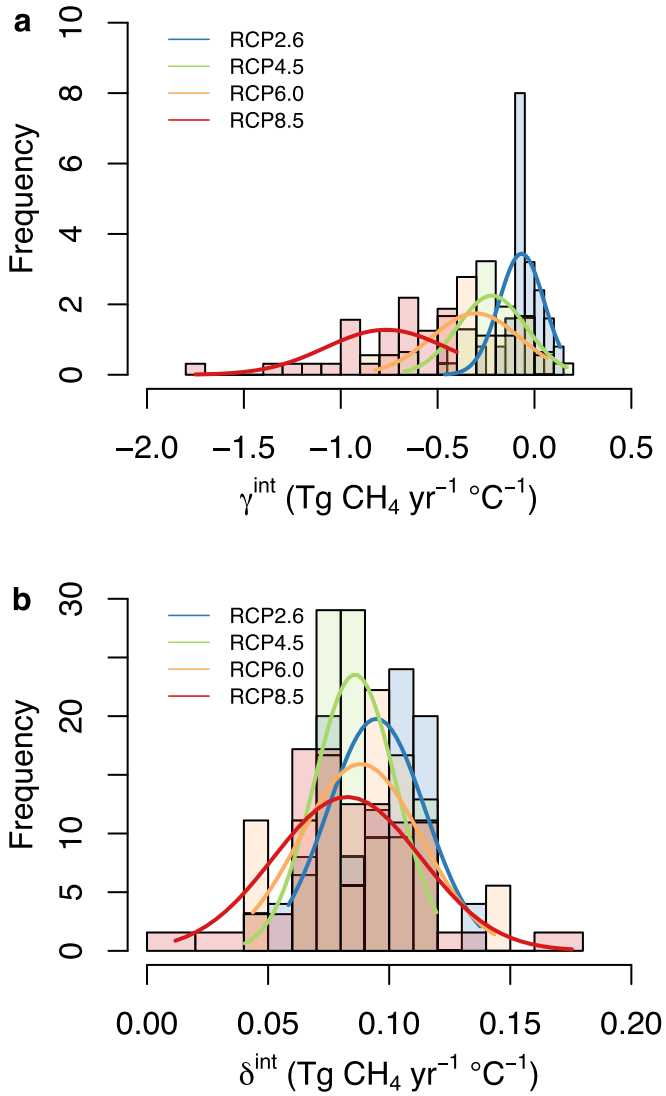
140

141 **Figure S5.** Annual variability of simulated wetland areal extent over major
142 boreal regions in future RCPs.



143

144 Figure S6. The comparison of time evolution of climate feedback parameter λ
145 between scenario with and without inclusion of wetland CH_4 feedback for each
146 RCP scenario. The feedback parameter (unit: W m^{-2} K^{-1}) is calculated as the ratio
147 of the change in global mean surface temperature to radiative flux at the top of
148 the atmosphere, assuming a linear energy balance model (31).



149

150 Figure S7. The response of global CH_4 emissions to (a) interannual variation in
151 temperature γ^{int}, and (b) interannual variation in precipitation δ^{int}.

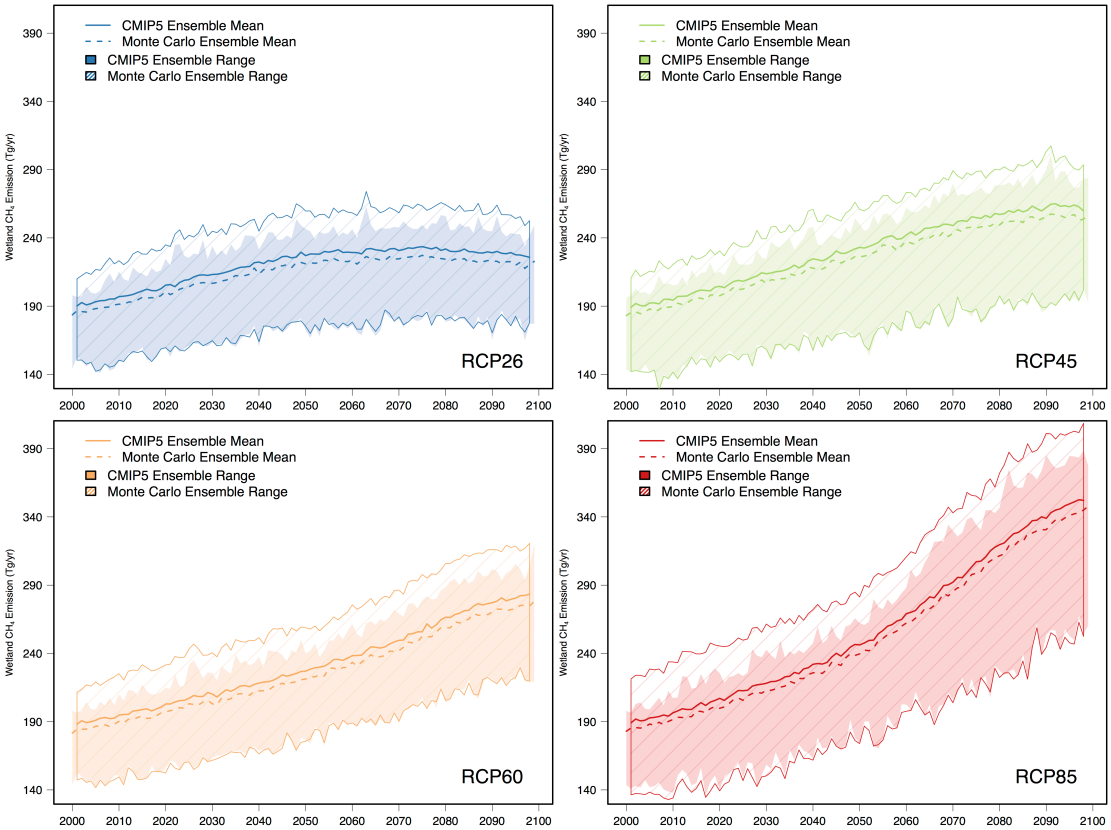


Figure S8. Time series of predicted future CH_4 emission from original CMIP5 simulations and Monte Carlo simulations based on a multiple linear regression approach.

References:

1. Spahni R, *et al.* (2011) Constraining global methane emissions and uptake by ecosystems. *Biogeosciences* 8(6):1643-1665.
2. Wania R, Ross I, & Prentice IC (2010) Implementation and evaluation of a new methane model within a dynamic global vegetation model: LPJ-WHyMe v1.3.1. *Geosci. Model Dev.* 3(2):565-584.
3. Zhang Z, Zimmermann NE, Kaplan JO, & Poulter B (2016) Modeling spatiotemporal dynamics of global wetlands: comprehensive evaluation of a new sub-grid TOPMODEL parameterization and uncertainties. *Biogeosciences* 13(5):1387-1408.
4. Cosby BJ, Hornberger GM, Clapp RB, & Ginn TR (1984) A Statistical Exploration of the Relationships of Soil Moisture Characteristics to the Physical Properties of Soils. *Water Resources Research* 20(6):682-690.
5. Lloyd J & Taylor JA (1994) On the Temperature Dependence of Soil Respiration. *Functional Ecology* 8(3):315-323.
6. Ringeval B, *et al.* (2012) Modelling sub-grid wetland in the ORCHIDEE global land surface model: evaluation against river discharges and remotely sensed data. *Geosci. Model Dev.* 5(4):941-962.
7. van Vuuren D, *et al.* (2011) RCP2.6: exploring the possibility to keep global mean temperature increase below 2°C. *Climatic Change* 109(1-2):95-116.
8. Piao S, *et al.* (2013) Evaluation of terrestrial carbon cycle models for their response to climate variability and to CO_2 trends. *Global Change Biology* 19(7):2117-2132.
9. Melton JR, *et al.* (2013) Present state of global wetland extent and wetland methane modelling: conclusions from a model inter-comparison project (WETCHIMP). *Biogeosciences* 10(2):753-788.
10. Zhu Q, *et al.* (2015) Estimating global natural wetland methane emissions using process modelling: spatio-temporal patterns and contributions to atmospheric methane fluctuations. *Global Ecology and Biogeography* 24:959-972.
11. Chen X, Bohn TJ, & Lettenmaier DP (2015) Model estimates of climate controls on pan-Arctic wetland methane emissions. *Biogeosciences* 12(21):6259-6277.
12. Zhu X, Zhuang Q, Lu X, & Song L (2014) Spatial scale-dependent land–atmospheric methane exchanges in the northern high latitudes from 1993 to 2004. *Biogeosciences* 11(7):1693-1704.
13. Meng L, *et al.* (2012) Sensitivity of wetland methane emissions to model assumptions: application and model testing against site observations. *Biogeosciences* 9(7):2793-2819.
14. Riley WJ, *et al.* (2011) Barriers to predicting changes in global terrestrial methane fluxes: analyses using CLM4Me, a methane biogeochemistry model integrated in CESM. *Biogeosciences* 8(7):1925-1953.
15. Glagolev M, Kleptsova I, Filippov I, Maksyutov S, & Machida T (2011) Regional methane emission from West Siberia mire landscapes. *Environmental Research Letters* 6(4):045214.
16. Melack JM, *et al.* (2004) Regionalization of methane emissions in the Amazon Basin with microwave remote sensing. *Global Change Biology* 10(5):530-544.

17. Zhuang Q, *et al.* (2004) Methane fluxes between terrestrial ecosystems and the atmosphere at northern high latitudes during the past century: A retrospective analysis with a process-based biogeochemistry model. *Global Biogeochemical Cycles* 18(3):GB3010.
18. Walter BP & Heimann M (2000) A process-based, climate-sensitive model to derive methane emissions from natural wetlands: Application to five wetland sites, sensitivity to model parameters, and climate. *Global Biogeochemical Cycles* 14(3):745-765.
19. Cao M, Marshall S, & Gregson K (1996) Global carbon exchange and methane emissions from natural wetlands: Application of a process-based model. *Journal of Geophysical Research: Atmospheres* 101(D9):14399-14414.
20. Christensen TR, Prentice IC, Kaplan J, Haxeltine A, & Sitch S (1996) Methane flux from northern wetlands and tundra. *Tellus B* 48(5):652-661.
21. Chang RY-W, *et al.* (2014) Methane emissions from Alaska in 2012 from CARVE airborne observations. *Proceedings of the National Academy of Sciences*.
22. Miller SM, *et al.* (2014) Observational constraints on the distribution, seasonality, and environmental predictors of North American boreal methane emissions. *Global Biogeochemical Cycles* 28(2):146-160.
23. Pickett-Heaps CA, *et al.* (2011) Magnitude and seasonality of wetland methane emissions from the Hudson Bay Lowlands (Canada). *Atmos. Chem. Phys.* 11(8):3773-3779.
24. Bousquet P, *et al.* (2011) Source attribution of the changes in atmospheric methane for 2006–2008. *Atmos. Chem. Phys.* 11(8):3689-3700.
25. Bloom AA, Palmer PI, Fraser A, Reay DS, & Frankenberg C (2010) Large-Scale Controls of Methanogenesis Inferred from Methane and Gravity Spaceborne Data. *Science* 327(5963):322-325.
26. Bousquet P, *et al.* (2006) Contribution of anthropogenic and natural sources to atmospheric methane variability. *Nature* 443(7110):439-443.
27. Chen Y-H & Prinn RG (2006) Estimation of atmospheric methane emissions between 1996 and 2001 using a three-dimensional global chemical transport model. *Journal of Geophysical Research: Atmospheres* 111(D10):2156-2202.
28. Mikaloff Fletcher SE, Tans PP, Bruhwiler LM, Miller JB, & Heimann M (2004) CH_4 sources estimated from atmospheric observations of CH_4 and its 13C/12C isotopic ratios: 1. Inverse modeling of source processes. *Global Biogeochemical Cycles* 18(4):1944-9224.
29. Wang JS, *et al.* (2004) A 3-D model analysis of the slowdown and interannual variability in the methane growth rate from 1988 to 1997. *Global Biogeochemical Cycles* 18(3):1944-9224.
30. Houweling S, Dentener F, & Lelieveld J (2000) Simulation of preindustrial atmospheric methane to constrain the global source strength of natural wetlands. *Journal of Geophysical Research: Atmospheres* 105(D13):17243-17255.
31. Knutti R & Rugenstein MAA (2015) Feedbacks, climate sensitivity and the limits of linear models. *Philosophical Transactions of the Royal Society A: Mathematical, Physical and Engineering Sciences* 373(2054).